

UC San Diego

UC San Diego Previously Published Works

Title

LRRK2 mediates axon development by regulating Frizzled3 phosphorylation and growth cone–growth cone communication

Permalink

<https://escholarship.org/uc/item/9p63h2jr>

Journal

Proceedings of the National Academy of Sciences of the United States of America, 117(30)

ISSN

0027-8424

Authors

Onishi, Keisuke

Tian, Runyi

Feng, Bo

et al.

Publication Date

2020-07-28

DOI

10.1073/pnas.1921878117

Copyright Information

This work is made available under the terms of a Creative Commons Attribution-NonCommercial-NoDerivatives License, available at <https://creativecommons.org/licenses/by-nc-nd/4.0/>

Peer reviewed



LRRK2 mediates axon development by regulating Frizzled3 phosphorylation and growth cone–growth cone communication

Keisuke Onishi^a, Runyi Tian^a, Bo Feng^a, Yiqiong Liu^a, Junkai Wang^a, Yinan Li^a, and Yimin Zou^{a,1}

^aNeurobiology Section, Biological Sciences Division, University of California San Diego, La Jolla, CA 92093

Edited by Carol Ann Mason, Columbia University, New York, NY, and approved June 9, 2020 (received for review December 13, 2019)

Axon–axon interactions are essential for axon guidance during nervous system wiring. However, it is unknown whether and how the growth cones communicate with each other while sensing and responding to guidance cues. We found that the Parkinson’s disease gene, leucine-rich repeat kinase 2 (*LRRK2*), has an unexpected role in growth cone–growth cone communication. The *LRRK2* protein acts as a scaffold and induces Frizzled3 hyperphosphorylation indirectly by recruiting other kinases and also directly phosphorylates Frizzled3 on threonine 598 (T598). In *LRRK1* or *LRRK2* single knockout, *LRRK1/2* double knockout, and *LRRK2 G2019S* knockin, the postcrossing spinal cord commissural axons are disorganized and showed anterior–posterior guidance errors after midline crossing. Growth cones from either *LRRK2* knockout or *G2019S* knockin mice showed altered interactions, suggesting impaired communication. Intercellular interaction between Frizzled3 and Vangl2 is essential for planar cell polarity signaling. We show here that this interaction is regulated by phosphorylation of Frizzled3 at T598 and can be regulated by *LRRK2* in a kinase activity-dependent way. In the *LRRK1/2* double knockout or *LRRK2 G2019S* knockin, the dopaminergic axon bundle in the midbrain was significantly widened and appeared disorganized, showing aberrant posterior-directed growth. Our findings demonstrate that *LRRK2* regulates growth cone–growth cone communication in axon guidance and that both loss-of-function mutation and a gain-of-function mutation (*G2019S*) cause axon guidance defects in development.

axon guidance | growth cone–growth cone interaction | Wnt/planar cell polarity | *LRRK2* | Frizzled3–Vangl2 interaction

During development, neuronal axons navigate in complex tissue terrains, steered by guidance molecules strategically placed in either a graded fashion or along sharp boundaries. Despite the successful identification of a large number of axon guidance molecules, our understanding of how growth cones detect and process these signals to make precise turning decisions remains limited (1). Most of the in vivo molecular gradients are apparently shallow. It is thought that a signal amplification mechanism would be necessary to detect subtle concentration differences and transform those into all-or-none turning decisions. Axons are known to interact with each other (2). Even less is known about the molecular signaling mechanisms that mediate axon–axon interactions and whether and how these interactions help establish the highly organized axon projections.

A large number of studies established that the Wnts are conserved guidance molecules for many neurons, controlling the direction of axon path finding as well as topographic mapping (3–12). Subsequent work showed that components of a non-canonical Wnt signaling pathway, planar cell polarity (PCP) pathway, function locally to polarize growth cones to steer axons (13–22). PCP is a conserved signaling pathway that conveys cell and tissue polarity along the tissue plane (23, 24). Six conserved core components (Frizzled [Fzd], Flamingo, Van Gogh [Vang], Prickle, Dishevelled [Dvl], and Diego) form dynamic and

asymmetric protein complexes. Although the signaling mechanisms have not been fully understood, the antagonistic interactions among the components appear to be a key substrate for creating or maintaining polarity. One such antagonistic interaction is between Dvl and Vang, whereby Dvl promotes Fzd3 cell surface localization and Fzd3 hyperphosphorylation but Vangl2 antagonizes Dvl1 (14). Another antagonism is between Dvl2 and Dvl1, whereby Dvl2 blocks the function of Dvl1 in inducing Fzd3 hyperphosphorylation and Fzd3 cell surface localization (17). These interactions among the Wnt–PCP signaling components, first discovered in rodents, were subsequently found to be conserved in *Caenorhabditis elegans* (25, 26).

Axons typically path find together in large and organized groups (2). However, it is unknown whether growth cones of the same cohort of axons communicate with each other during path finding. PCP signaling depends on the interactions among the cells that are being polarized (23, 24). PCP components are known to form intercellular complexes, involving Flamingo, Fzd and Dvl on the distal plasma membrane of each cell and Flamingo, Vang, and Prickle on the proximal plasma membrane of the neighboring cell. Such intercellular interactions are postulated to initiate, amplify, or maintain the polarity signals. In particular, the intercellular transinteraction between Fzd and Vang is a key step in this essential process of PCP signaling (27).

Significance

In addition to responding to directional cues, axons join one another as they extend to form highly organized projections. We show here that growth cones communicate with each other, and this communication is mediated by planar cell polarity signaling components, which are known to mediate cell–cell interactions in tissue polarization. This interaction is, in part, mediated by an intercellular interaction between Frizzled3 and Vangl2. Leucine-rich repeat kinase 2 (*LRRK2*), encoded by a Parkinson’s disease gene, regulates Frizzled3 phosphorylation and the intercellular interaction between Frizzled3 and Vangl2. Both loss-of-function and gain-of-function *LRRK2* mutants show axon guidance defects, including those of the dopaminergic neurons, suggesting that this Parkinson’s disease gene plays important roles in growth cone–growth cone interactions during axon development.

Author contributions: K.O. and Y.Z. designed research; K.O., R.T., B.F., Y. Liu, J.W., and Y. Li performed research; Y.Z. analyzed data; and K.O., R.T., and Y.Z. wrote the paper.

Competing interest statement: Y.Z. is the founder of VersaPeutics and has equity, compensation, and interim managerial role. The terms of this arrangement have been reviewed and approved by the University of California San Diego in accordance with its conflict of interest policies.

This article is a PNAS Direct Submission.

This open access article is distributed under [Creative Commons Attribution-NonCommercial-NoDerivatives License 4.0 \(CC BY-NC-ND\)](https://creativecommons.org/licenses/by-nc-nd/4.0/).

¹To whom correspondence may be addressed. Email: yzou@ucsd.edu.

This article contains supporting information online at <https://www.pnas.org/lookup/suppl/doi:10.1073/pnas.1921878117/-DCSupplemental>.

First published July 8, 2020.

While searching for regulators of Fzd3 phosphorylation, we discovered that Leucine-rich repeat kinase 2 (LRRK2) acts as a scaffold to induce Fzd3 hyperphosphorylation by recruiting other kinases and can directly phosphorylate Fzd3 on threonine 598. We created *LRRK1* and *LRRK2* knockout mice using the clustered regulatory interspaced short palindromic repeats-CRISPR-associated 9 (CRISPR-Cas9) system and found that *LRRK1/LRRK2* single and double knockouts (DKO) caused major disorganization of post-crossing commissural axons, including anterior-posterior (A-P) guidance errors. The gain-of-function *LRRK2* mutant (*G2019S*) also displayed similar guidance defects. The A-P directional defects were not as severe as mutations of the core PCP proteins, such as the *Dvls*, suggesting that the main function of *LRRK1/2* may be to regulate growth cone-growth cone interaction to enhance the fidelity of guidance. Growth cones from *LRRK2* knockout (KO) or *LRRK2 G2019S* showed reduced ability to form stable contacts, suggesting less effective communication. To test how Fzd3 phosphorylation regulates intercellular interactions, we established a transcellular interaction assay. Cells were transfected with either *Celsr3/Fzd3* or *Celsr3/Vangl2* separately and cultured for one day and then mixed together and cultured for one more day. We then tested whether Fzd3 and Vangl2 can interact with each other in trans by using coimmunoprecipitation assay. We observed that *Celsr3* promotes the in trans interaction between Fzd3 and Vangl2 but phosphorylation of T598 on Fzd3 inhibits the trans interaction between Fzd3 and Vangl2. Furthermore, phosphorylation of T598 on Fzd3 promotes the in cis interaction between Fzd3 and *Celsr3*, which may be the cause of reduced Fzd3-Vangl2 in trans interactions. Using the same transcellular interaction assay, we found that overexpression of *LRRK2* wild type (WT) and *G2019S* caused a reduction of Fzd3-Vangl2 interaction but the kinase null *LRRK2* did not, suggesting that the kinase activity of *LRRK2* is required for regulating the Fzd3-Vangl2 intercellular interaction. Finally, *LRRK1* and *LRRK2* double knockout or *LRRK2 G2019S* gain-of-function mutation led to the widening of the midbrain dopaminergic (mDA) neuron axon bundle and A-P guidance errors.

Results

LRRK2 Directly Phosphorylates Fzd3 on T598 and Indirectly Promotes Dvl1-Induced Fzd3 Hyperphosphorylation. In order to understand how PCP signaling regulates growth cone turning, we set out to identify the kinases that phosphorylate Fzd3. We showed previously that Dvl1 can induce Fzd3 phosphorylation on at least seven sites in its cytoplasmic tail (S509, T543, T562, S577, S588, S625, and S637) (*SI Appendix, Fig. S1A*) (14, 17). One possibility is that multiple kinases are recruited by Dvl1 and phosphorylate Fzd3 sequentially. Another possibility is that a scaffold protein, recruited by Dvl1, may bring multiple kinases close to Fzd3 and phosphorylate Fzd3 (*SI Appendix, Fig. S1B*). Among the candidates we tested, *LRRK2*, a Dvl-interacting protein (28), is particularly relevant. *LRRK2* is either shown or proposed to interact with a number of kinases, many of which are putative Fzd3 kinases based on their consensus sequences (*SI Appendix, Fig. S1A*) (29–35). We first tested whether *LRRK2* is required for Dvl1-induced Fzd3 hyperphosphorylation in HEK293 cells. We developed two shRNAs targeting human *LRRK2* (Fig. 1A). We observed indeed that *LRRK2* knockdown led to a significant reduction of Dvl1-induced Fzd3 hyperphosphorylation (Fig. 1B and C).

Because *LRRK2* is also a kinase, we then tested whether *LRRK2* can directly phosphorylate Fzd3 using an in vitro kinase assay. To better resolve phosphorylation, we utilized the phosphate-binding tag (Phos-tag) system, which enhances phosphorylation-derived mobility shift using selective Phos-tag (36). We tested three forms of *LRRK2* recombinant proteins: WT, *G2019S*, or kinase negative (KN; D1994A). *G2019S* (*GS*) is one of the most frequent *LRRK2* mutations in Parkinson's disease patients with an enhanced kinase activity of *LRRK2* (37, 38). The *LRRK2* proteins (WT, *GS*, or KN) did not induce mobility shift of glutathione

S-transferase (*GST*) alone. In contrast, *LRRK2* WT or *GS*, but not *LRRK2* KN, induced mobility shift of glutathione S-transferase-Fzd3 cytoplasmic domain fusion protein (*GST-Fzd3cyto*) (Fig. 1D). Using liquid chromatography mass spectrometry (LC-MS/MS) (39, 40), we found that *LRRK2* phosphorylates Fzd3 on T598 (Fig. 1E). This is a site in addition to the seven sites we previously identified.

We then tested how *LRRK2* regulates Fzd3 phosphorylation. As expected, we observed that *LRRK2* WT and *LRRK2* *GS* further enhance Dvl1-induced Fzd3 phosphorylation and cell surface accumulation using cell surface biotinylation assay (Fig. 1F–H). Interestingly, *LRRK2* KN also enhances Dvl1-induced Fzd3 phosphorylation and cell surface accumulation (Fig. 1F–H), indicating that *LRRK2* also functions as a scaffold protein to recruit other kinases for Fzd3 phosphorylation on those seven sites. This also suggests that *LRRK2* is not a priming kinase for the other seven sites.

We sought to better understand the relationship between Fzd3 phosphorylation and Fzd3 cell surface localization. We previously showed glycosylation is required for Fzd3 cell surface localization (41). Using glycosylation-deficient Fzd3 (N356Q and 2NQ [N42Q + N356Q]), we found that N356Q and 2NQ mutants are not hyperphosphorylated in the total cell extracts (*SI Appendix, Fig. S2A and B*), suggesting that cell surface localization is necessary for Fzd3 hyperphosphorylation. Consistent with this result, Dvl1 expression did not induce Fzd3 hyperphosphorylation of N356Q and 2NQ mutants (*SI Appendix, Fig. S2C and D*). These results suggest that the Fzd3 kinases are either on the plasma membrane or close to the plasma membrane.

We then asked whether Fzd3 phosphorylation is required for its plasma membrane localization. The phosphorylation-mutant forms of Fzd3, T598A, 7A, and 8A (T598A combined with 7A) were found expressed on the cell surface (*SI Appendix, Fig. S2C and D*). Furthermore, Dvl1 was still able to promote the hyperphosphorylation of these mutant forms of Fzd3. We reported previously that the nonphosphorylated Fzd3 binds to ADP-ribosylation factor 6 (Arf6), which promotes Fzd3 endocytosis (17). Taken together, these results indicate that Fzd3 is first recruited to the cell surface by Dvl1 and *LRRK2* and then hyperphosphorylated by other kinases as well as *LRRK2* itself (*SI Appendix, Fig. S2E*). Additionally, phosphorylation of Fzd3 helps retain Fzd3 on the plasma membrane by reducing Arf6-mediated endocytosis.

Axon Guidance Defects of Spinal Cord Commissural Neurons in *LRRK* Mutants. In a previous RNA-sequencing experiment, we observed that *LRRK2* messenger RNA (mRNA) was expressed in the dorsal spinal cord at E11.5 [FKPM (fragments per kilobase of exon per million mapped fragments) = 0.36 (41)]. Using in situ hybridization, we now confirmed the expression of *LRRK2* in the spinal cord (*SI Appendix, Fig. S3A and B*). As *LRRK1* is also expressed [FKPM = 0.62 (41)] and *LRRK1* shares sequence homology and a similar domain organization, *LRRK1* may have redundant functions as *LRRK2* (42). We therefore generated knockout alleles of *LRRK2* and *LRRK1* using the CRISPR-Cas9 system. We prepared two sgRNAs targeting intron1 and intron2 to excise exon2, resulting in a frame shift and null allele of *LRRK2* (*SI Appendix, Fig. S3C–E*). For *LRRK1*, we prepared two sgRNAs targeting intron3 and intron5 to excise exon4 and exon5, resulting in a frame shift (*SI Appendix, Fig. S3F and G*). In order to avoid potential off-target effects, we back crossed *LRRK2* and *LRRK1* KO into the WT B6 background for six generations and then crossed them together for double knockout. To confirm that *LRRK2* does regulate Fzd3 in vivo, we extracted proteins from dorsal spinal cord tissue from E11.5 embryos. We observed decreased levels of Fzd3 phosphorylation as *LRRK2* was removed (*SI Appendix, Fig. S3H*). Comparing lanes 2 and 3, loss of *LRRK2* led to a decrease of Fzd3 hyperphosphorylation in vivo (*SI Appendix, Fig. S3H*).

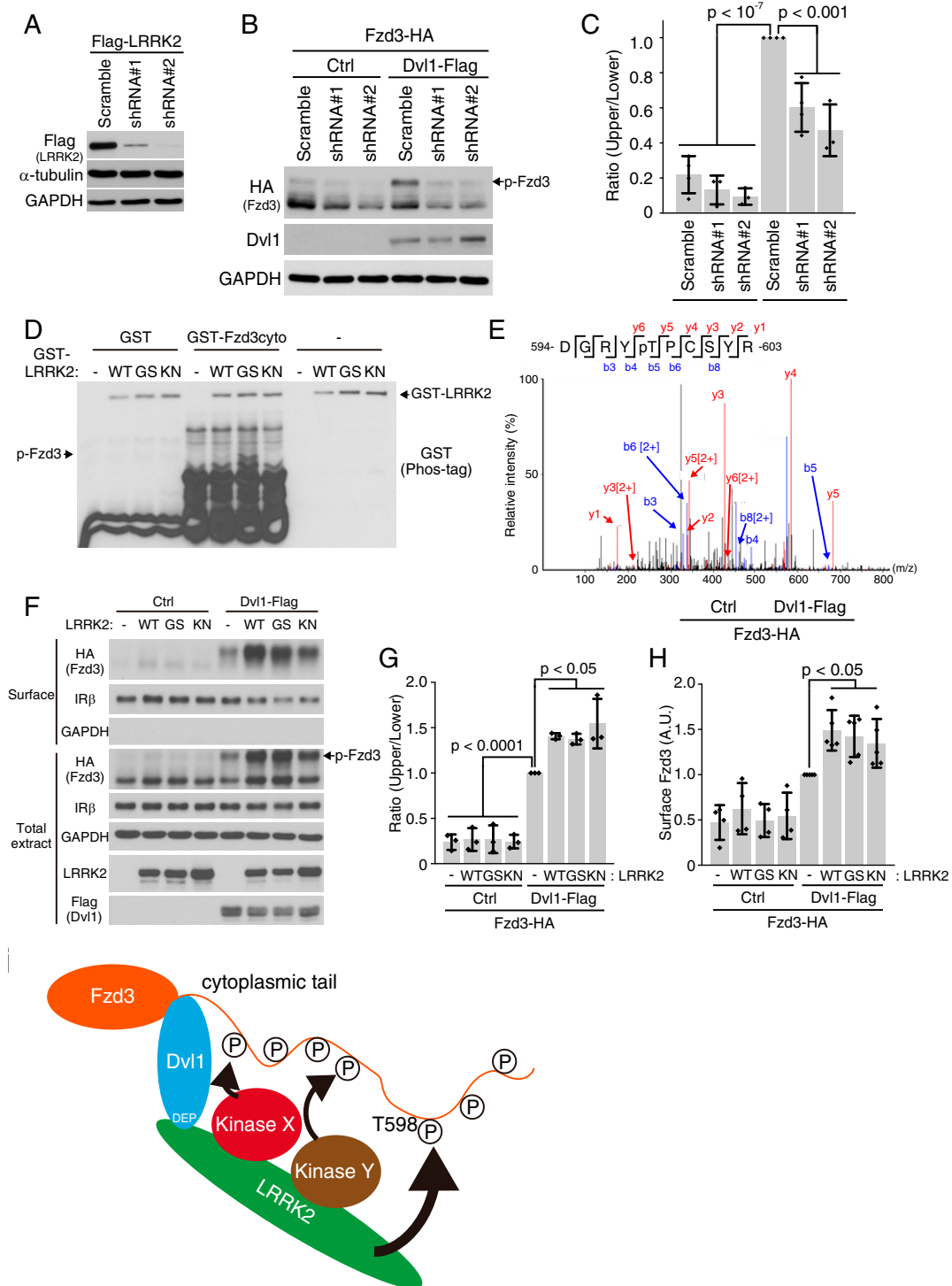


Fig. 1. LRRK2 directly phosphorylates Fzd3 and also promotes Fzd3 phosphorylation by acting as a scaffold. (A) Validation of two shRNAs that target the human LRRK2 by western blotting. (B) Immunoblots showed that knocking down LRRK2 reduced Dvl1-induced Fzd3 phosphorylation. Black arrow indicates hyperphosphorylated Fzd3 band. (C) Quantification of the extent of Fzd3 hyperphosphorylation in B. Four independent experiments were performed, and results were plotted as individual data points. The data are mean \pm SD. One-way ANOVA with post hoc Tukey test was used for statistics. (D) LRRK2 directly phosphorylates the cytoplasmic region of Fzd3 in an *in vitro* kinase assay. Phosphorylation is analyzed using the Phos-tag SDS/PAGE. WT recombinant LRRK2 and LRRK2 G2019S (GS) induced mobility shift of GST-Fzd3cyto, while control (no kinase) and KN did not. Black arrow indicates phosphorylated Fzd3 band. (E) The mass spectrum of phosphorylated peptide from Fzd3. Phosphorylation on threonine 598 site was detected. (F) LRRK2 enhanced Dvl1-induced Fzd3 phosphorylation and cell surface accumulation in a kinase activity-independent manner. G and H are quantifications of F. Data are presented as mean with SD. Diamond dots indicate kinase activity-independent experimental data points (three independent experiments were quantified for phosphorylation, five independent experiments were quantified for Fzd3 cell surface localization). One-way ANOVA with post hoc Tukey test was used for statistics. (I) Regulation of Fzd3 phosphorylation by the Dvl1-LRRK2. LRRK2 directly phosphorylates Fzd3 at T598. Meanwhile, LRRK2 functions as a scaffold protein to bring other kinases to induce Fzd3 hyperphosphorylation in a kinase-activity independent manner. Ctrl, control. HA, human influenza hemagglutinin. SDS/PAGE, sodium dodecyl sulfate/polyacrylamide gel electrophoresis. GAPDH, glyceraldehyde 3-phosphate dehydrogenase.

To visualize commissural axons in vivo, we labeled the dorsal commissural (dl1) neurons by crossing the *Atoh1-CreER^{T2}* with the *Ai9* reporter line, as *Atoh1* (Atonal bHLH transcription factor 1) is specifically expressed in the progenitor cells of the dl1 neurons. Upon activation, the *Ai9* reporter, with a CAG-loxP-STOP-loxP-tdTomato cassette in the *Gt (Rosa)26Sor* locus, will express tdTomato and label the axonal projections. *LRRK1* and *LRRK2* KO mice were crossed with the *Atoh1-CreER^{T2}/Ai9* tdTomato mice. Tamoxifen was intraperitoneally injected in pregnant female mice at E9.5. Embryos were then collected at E11.5, and “open-book” spinal cords were prepared for staining and imaging (Fig. 2A). The *Atoh1*-positive neurons project axons anteriorly at an angle after their axons have crossed the floor plate. This allows us to clearly observe their overall organization as well as the direction of turning after midline crossing (Fig. 2B) (43, 44). To more clearly visualize the direction of axon turning and organization, we sparsely labeled axons by injecting lower doses of tamoxifen (Fig. 2B).

In the *WT* spinal cords, the tdTomato-positive dl1 axons crossed the floor plate and turned anteriorly in a highly organized way. On the other hand, in the *LRRK2* KO, the dl1 axons are severely disorganized and wandered after crossing floor plate (Fig. 2C). Some axons turned to grow posteriorly, instead of anteriorly. In *LRRK1* KO, we observed milder guidance defects.

LRRK1/2 DKO showed slightly stronger guidance defects than *LRRK2* KO alone, suggesting that *LRRK2* may be the main *LRRK* in these commissural neurons at this stage of development (Fig. 2C). Taken together, these results indicate that both *LRRK1* and *LRRK2* are required for postcrossing guidance of dl1 axons in the developing spinal cord. Compared with *Fzd3* knockout (3), the A–P directional defects in *LRRK2* single or *LRRK1/2* double knockouts appear to be less severe, suggesting that the main function *LRRK1/2* is to mediate growth cone–growth cone interaction, which may be required for high-fidelity A–P guidance.

To test the role of proper levels of *Fzd3* phosphorylation, we set out to analyze *LRRK2 GS*, which has enhanced kinase activity. We analyzed commissural axon projections in *LRRK2 GS* knockin mice using the lipophilic dye I (diI) and observed similar axon disorganization phenotype with A–P guidance defects (Fig. 3). In *WT* control, the axons are highly organized, grow across the midline, and turn anteriorly along straight paths (labeled green in Fig. 3A). The green axons grow along straight lines, gradually away from the midline after crossing, suggesting proper coordination among axons. However, in *LRRK2 GS* knockin mice, axons were disorganized, with some showing wavy paths (labeled blue in Fig. 3A). These blue axons do not follow a

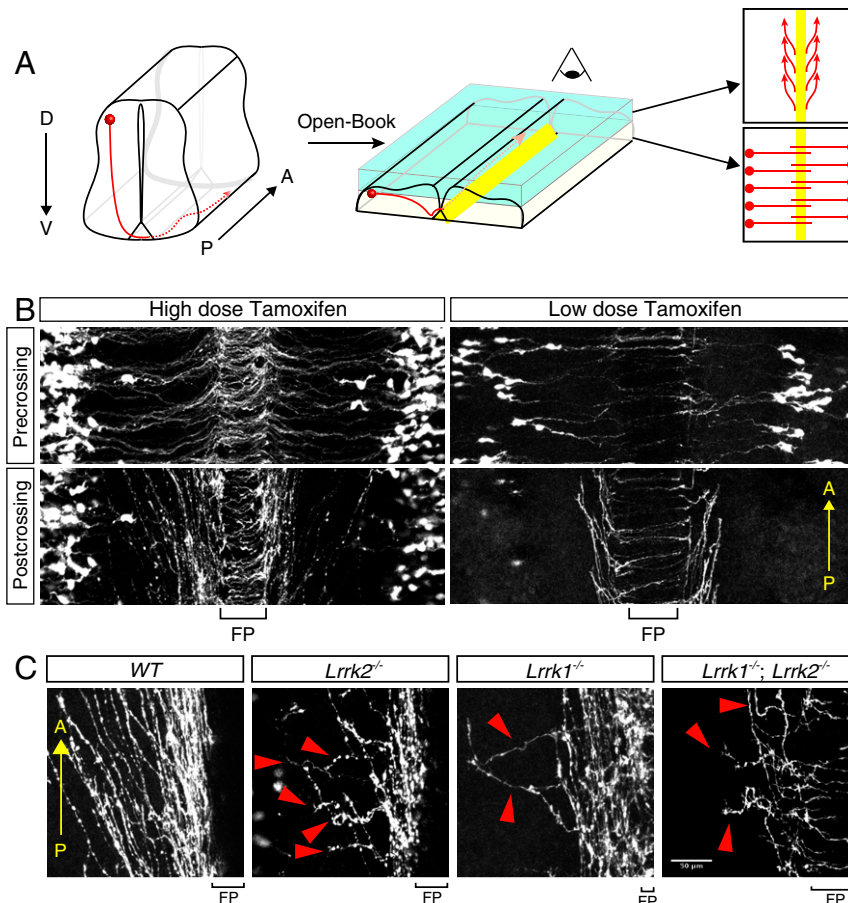


Fig. 2. *LRRK1/2* are required for postcrossing guidance of dl1 commissural axons. (A) Diagram showing the trajectory of the dl1 axons in the open-book spinal cord view. E11.5 dl1 axons (red line) were visualized by *Atoh1-CreER^{T2}/Ai9* tdTomato. The box in *Upper Right* shows the trajectory of the *Atoh1*⁺ axons. Because of the three-dimensional structure of the spinal cord, the precrossing and postcrossing segments of the commissural axons are located on different focal planes. A, anterior; D, dorsal; P, posterior; V, ventral. (B) TdTomato signal shows the trajectory of the *WT* *Atoh1*⁺ commissural axons with dense or sparse labeling. “Precrossing” is the focal plane that shows the precrossing segment. “Postcrossing” is the focal plane that shows the crossing and postcrossing segments. (C) *LRRK1/2* are required for both the organization and direction of turning of dl1 commissural axons after midline crossing. In *LRRK1* and *LRRK2* single-KO or *LRRK1/2* DKO spinal cords, tdTomato-positive dl1 commissural axons showed highly disorganized trajectory as well as abnormal posterior turning (indicated with red arrowheads). FP, floor plate. (Scale bar, 50 μ m.)

straight path and often grow along the midline rather than away from the midline. In *LRRK2* GS knockin mice, some axons turned posteriorly (labeled red in Fig. 3A).

Severe A–P Guidance Defects in *Dvl2* Single and *Dvl1/3* Double Mutants. To further test the notion that the main function of LRRK2 is to mediate growth cone–growth cone interactions to enhance the fidelity of A–P guidance, we analyzed the mutations of another PCP component, the Dvl. We reported previously that *Dvl1* and *Dvl3* promote Fzd3 phosphorylation, whereas *Dvl2* antagonizes *Dvl1* and *Dvl3* (17). Based on our hypothesis that proper levels of Fzd3 phosphorylation are essential for its traffic and function, we predict that both *Dvl1/3* and *Dvl2* should be required for A–P guidance of commissural axons. We prepared open-book spinal cords from E11.5 mouse embryos, and commissural axons were visualized using iontophoretic injection of DiI (*SI Appendix*, Fig. S4). Commissural axons turned anteriorly normally in *Dvl1* or *Dvl3* single KO. On the other hand, in *Dvl1/3* DKO, commissural axons turned randomly along the A–P axis (Fig. 4A and B). We also tested the necessity of *Dvl1/3* using the genetic-labeling method as we described above (Fig. 2A). In *Dvl1* single KO, tdTomato-positive dI1 axons crossed the floor plate, turning anteriorly and departing from the floor plate (Fig. 4C). This is the typical trajectory of the dI1 axons (43, 44). In *Dvl1/3* DKO, tdTomato-positive dI1 axons still cross floor plate. However, the postcrossing axons turned randomly along the A–P axis (Fig. 4C). In addition to the strong disorganization, direction of turning along the A–P axis is completely random, much stronger than the LRRK mutants (Figs. 2 and 3).

Next, we tested whether *Dvl2* is also required for the A–P guidance of commissural axons using a *Dvl2* floxed allele crossed with *Wnt1-Cre* (45–47). We confirmed that *Dvl2* protein level

was robustly reduced in the dorsal spinal cord of *Dvl2* cKO (Fig. 4D). We then analyzed spinal cord commissural axon trajectory using DiI tracing and found that commissural axons turned completely randomly along the A–P axis in *Dvl2* cKO (Fig. 4E and F). Compared with the LRRK mutants, the A–P directional phenotypes in mutants of the core PCP components, such as *Dvls* shown here and *Fzd3*, *Celsr3*, and *Vangl2* shown previously, are more severe, with ~50% of the axons turning posteriorly. This suggests that LRRK-mediated Fzd3 phosphorylation may be primarily responsible for regulating proper growth cone–growth cone interactions to increase the precision of turning. The other aspects of Fzd3 functions are not dependent on LRRK.

LRRK2 Regulates Growth Cone–Growth Cone Communication. In order to analyze growth cone–growth cone communication, we established a dissociated culture system for spinal cord commissural neurons. E11.5 mouse embryos were dissected, and commissural neurons from the dorsal margin of the spinal cord (one-fifth to one-fourth) were dissociated and cultured. After 24 h, axons with evident growth cones can be visualized; 48 h after culture, the majority of protrusions merged together to form axon bundles. We therefore started time-lapse imaging 30 h after the start of the culture to capture growth cone–growth cone interactions before the axons merge. In the control group, most growth cones merge quickly after they get close to each other and after their filopodia first contacted, forming stable axon bundles (Fig. 5A and *Movie S1*). The interval between first contact and merge is less than 5 min, which we classify as “determined” (Fig. 5A). However, in LRRK2 KO groups, many growth cone pairs separated after their filopodia first contact and repeatedly contacted one another, failing to form stable bundles

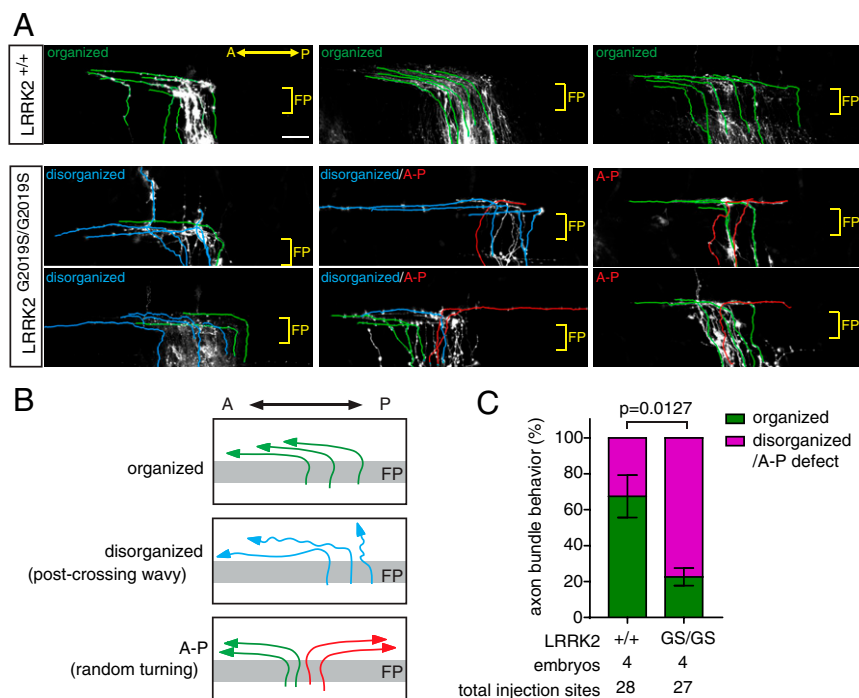


Fig. 3. Commissural axon guidance defects in LRRK2 GS embryos. (A) Commissural axons labeled by lipophilic DiI in E11.5 dorsal spinal cord. Axons were automatically traced using the Imaris software. The green lines indicate the organized anterior turning axons. The blue lines indicate the disorganized/waving axons. The red lines indicate the posterior turning axons. (Scale bar, 50 μ m.) (B) Illustration of axon projections revealed by DiI injection. “Organized” means that all axons turned anteriorly in an organized and straight way. “Disorganized” means that some axons were not straight after midline crossing. “A–P” means that axons turned anteriorly and posteriorly randomly. (C) Quantification of axon projections revealed by DiI injections in A. The graph represents the percentage of injection sites showing organized, disorganized, or A–P trajectory. Data are presented as mean \pm SEM. Student’s *t* test (two-tailed distribution) was used for statistics. A, anterior; A–P, anterior–posterior guidance defect; FP, floor plate; P, posterior.

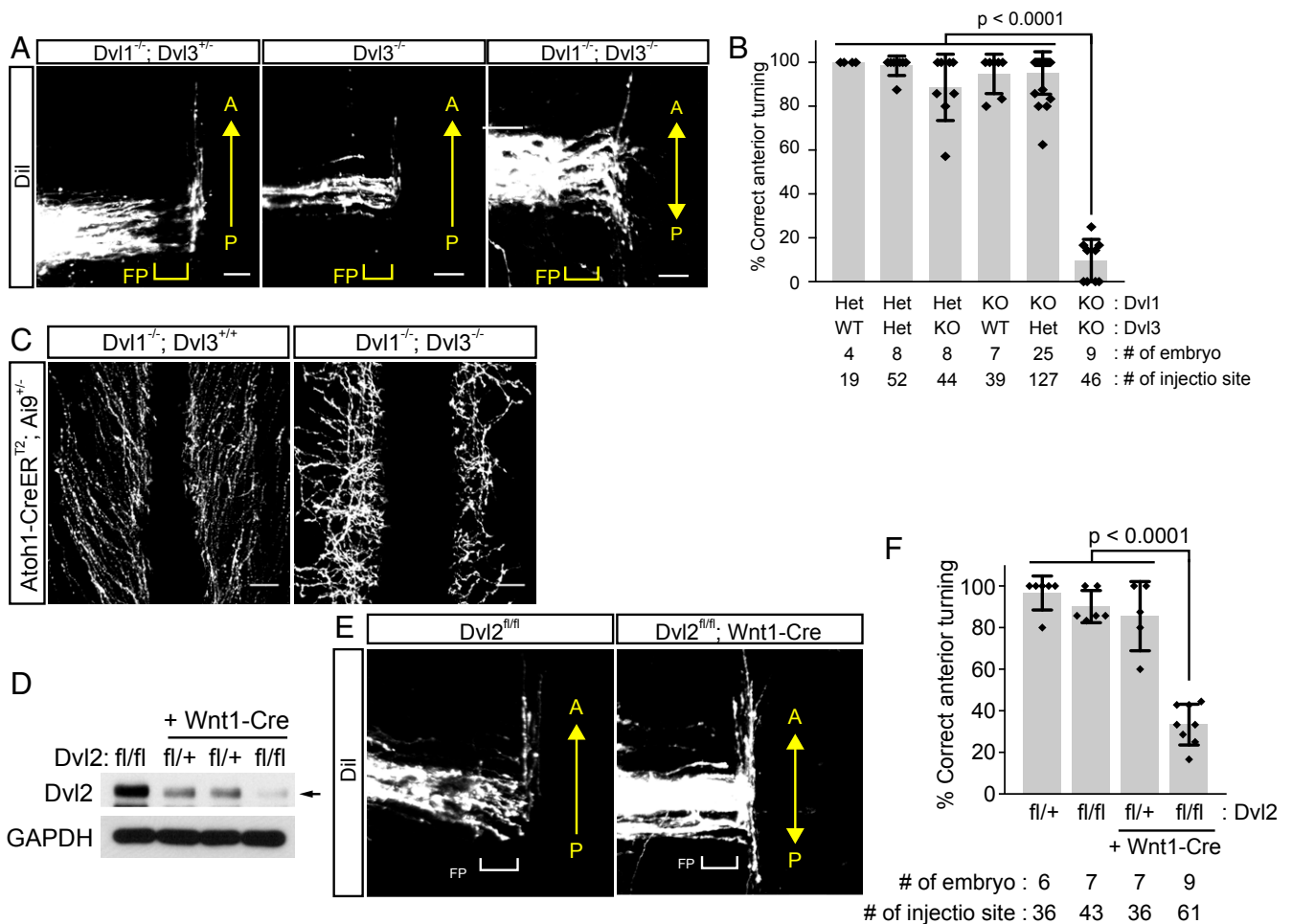


Fig. 4. Strong A–P guidance defects of commissural axons in *Dvl* mutants. (A) Strong A–P guidance defects in *Dvl1*^{−/−}; *Dvl3*^{−/−}. Commissural axons were labeled by Dil injection into the dorsal margin of the spinal cord. (Scale bars, 50 μm.) (B) Quantification of the A–P guidance defects in A. The graph represents the percentage of injection sites showing normal (correct) anterior turning. Gray bars indicate means of all data points. Black bars indicate SDs. Each diamond dot indicates one embryo. One-way ANOVA with post hoc Tukey test was used for statistics. (C) A–P guidance defects of dl1 commissural axons after midline crossing. dl1 axons were labeled using the *Atoh1-CreER*^{T2} line crossed with the *Ai9* tdTomato reporter line. Postcrossing dl1 axons in control (*Dvl1*^{−/−}; *Dvl3*^{+/+}) turned anteriorly along the A–P axis (Left), whereas dl1 axons in double knockout (*Dvl1*^{−/−}; *Dvl3*^{−/−}) turned randomly along the A–P axis (Right). (Scale bars, 50 μm.) (D) *Dvl2* protein levels in the dorsal spinal cord of the *Dvl2* cKO (*Wnt1-Cre*). Black arrow indicates *Dvl2* bands. (E) A–P guidance defects of commissural axons in *Dvl2* cKO. Commissural axons were labeled by lipophilic Dil injection into the dorsal margin of the spinal cord. (Scale bars, 50 μm.) (F) Quantification of A–P guidance defects in E. The graph represents the percentage of injection sites showing normal (correct) anterior turning. Data are presented as mean with SD. Diamond dots in graph indicate individual data points of embryos. One-way ANOVA with post hoc Tukey test was used for statistics. A, anterior; FP, floor plate; P, posterior; GAPDH, glyceraldehyde 3-phosphate dehydrogenase.

(Fig. 5A and Movie S2). We classified this behavior “hesitant” (Fig. 5C). In the control group, $72.79 \pm 3.66\%$ of the growth cone pairs showed determined behavior, whereas only $47.46 \pm 3.93\%$ of the *LRRK2*-deficient growth cone pairs showed determined behavior. The increased proportion of hesitant behavior in *LRRK2* KO suggests abnormal growth cone–growth cone communications (Fig. 5D). We focused on the growth cone–growth cone interactions when two axons were meeting from neuron cell bodies at different locations in order to image and quantify their interactions. In the developing spinal cord *in vivo*, large numbers of commissural axons would be growing across the midline from the same side of the spinal cord and turn anteriorly together.

Similar to the loss-of-function mutation, the growth cone pairs with *LRRK2* gain-of-function mutation, GS, also showed separation after their first contact (Fig. 6B and Movies S3 and S4). There was a significant reduction of determined behavior in the *LRRK2*^{GS/GS} growth cones ($43.42 \pm 5.62\%$) compared with their

WT littermates ($74.26 \pm 7.43\%$) (Fig. 5D). These similar phenotypes of *LRRK2* KO and GS suggests that proper levels of *LRRK2* kinase activity are required for normal growth cone–growth cone communication.

The Phosphorylation State of *LRRK2* on T598 Regulates the Intercellular Interaction between *Fzd3* and *Vangl2*. To understand whether and how *Fzd3* phosphorylation may affected growth cone–growth cone communications, we set out to test the protein–protein interactions among PCP components, particularly the intercellular interactions. PCP signaling transduces directional information across cells through the core PCP proteins, such as *Fleming*/*Celsr*, *Vang*/*Vangl*, and *Fzd* (48). Among these three proteins, the *Fzd*–*Vang* intercellular interaction is thought to be important to transduce polarity signaling. Thus far, several reports showed that *Fzd* and *Vangl* are colocalized at cell–cell boundaries in the *Drosophila* wing epithelia and in the mouse cochlea (48). However, little is known how this interaction is

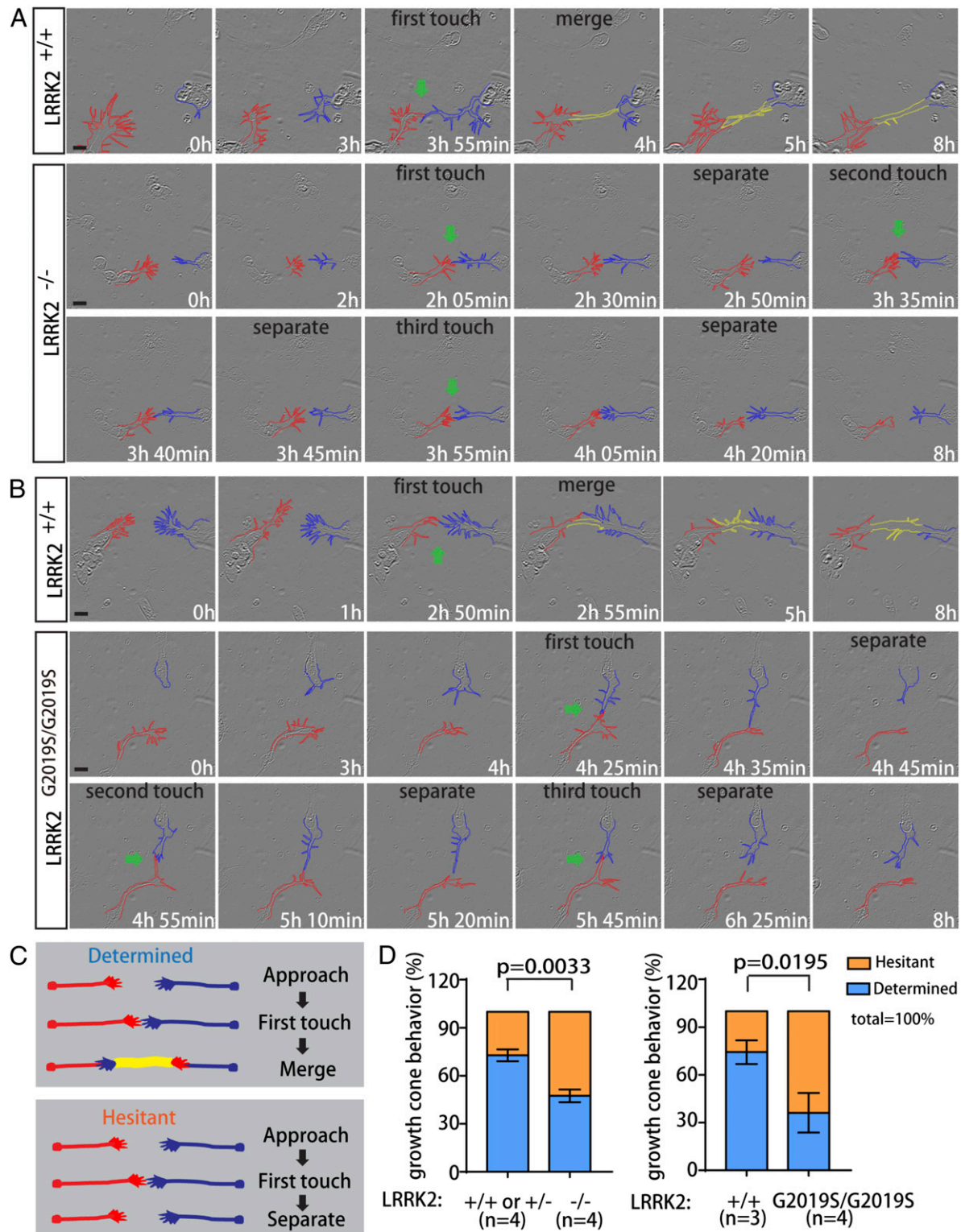


Fig. 5. LRRK2 regulates growth cone–growth cone interaction. (A) Time-lapse imaging of cultured commissural neurons from *LRRK2* knockout or WT embryos. Growth cones, which were contacting each other, were labeled with red and blue dash lines. Yellow dash lines outline the overlapped segment after two axons merge. Green arrows indicate the timepoints when two growth cones start to contact each other. Labeled time points are from the start of imaging. (Scale bars, 10 μ m.) (B) Time-lapse imaging of cultured *LRRK2*^{G2019S} or WT commissural neurons. (Scale bars, 10 μ m.) (C) Schematics of growth cone–growth cone interaction. Two pairs of commissural axon growth cones were drawn in red and blue. Yellow line indicates the overlapped segment after two axons merge. Determined: growth cones and axons merge rapidly after first touch. Hesitant: growth cones separate after first touch and repeatedly contact each other. (D) Quantification of growth cone–growth cone interactions in A and B. *n* represents the number of embryos. Embryos were collected from three different litters. Data are presented as mean \pm SEM. Student's *t* test (two-tailed distribution) was used for statistics.

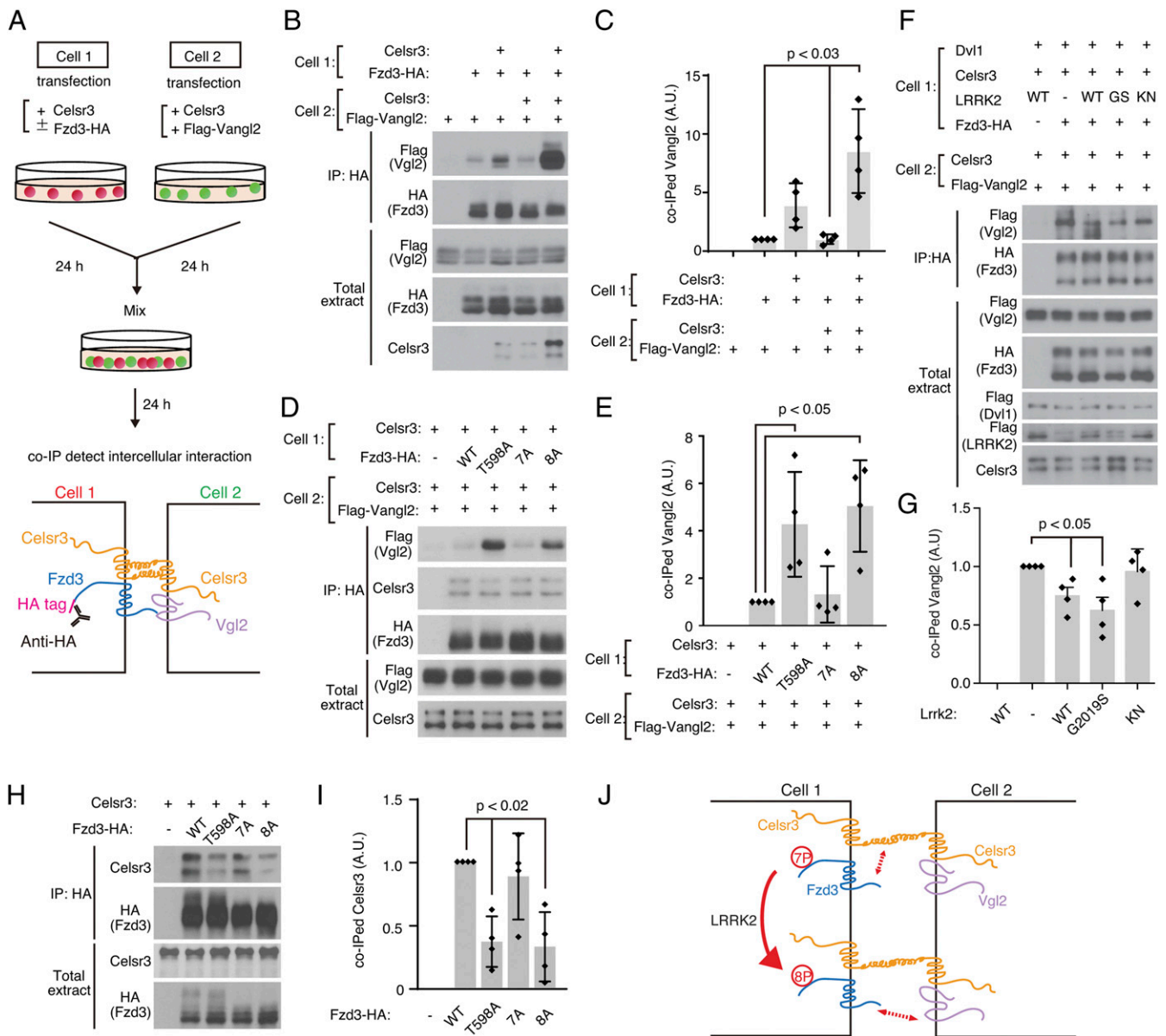


Fig. 6. Intercellular interaction between Fzd3 and Vangl2 is regulated by Fzd3 phosphorylation on T598 and by LRRK2 in a kinase activity-dependent manner. (A) Schematics of the transcellular interaction assay. Cells were seeded on separate plates, followed by transfection of indicated plasmids. After 24-h incubation, cells were dissociated, mixed, and cultured together. Coimmunoprecipitations were performed to test the intercellular complex of Fzd3 and Vangl2. (B) Celsr3 promoted the interaction between Fzd3 and Vangl2 detected by cell-mixing assay. (C) Quantification of coimmunoprecipitated Vangl2 in B. Each data point represents one independent experiment. Four independent experiments were performed. Data were represented as mean with SD. One-way ANOVA with post hoc Tukey test was used for statistics. (D) Increased Fzd3–Vangl2 intercellular interaction when Fzd3 phosphorylation site was mutated on T598. (E) Quantification of D. Gray bars indicate the mean of all data points. Black bars indicate SDs. Diamond dots indicate individual data points. Four independent experiments were performed. One-way ANOVA with post hoc Tukey test. (F) LRRK2 inhibits Fzd3–Vangl2 intercellular interaction in a kinase dependent manner. (G) Quantification of F. Gray bars indicate the mean of all data points. Black bars indicate SDs. Diamond dots indicate individual data points. Four independent experiments were performed. One-way ANOVA with post hoc Tukey test. (H) Decreased Fzd3–Celsr3 complex formation when Fzd3 phosphorylation site was mutated on T598. (I) Quantification of coimmunoprecipitated Celsr3 in H. Each data point represents one independent experiment. Data were represented as mean with SD. One-way ANOVA with post hoc Tukey test. (J) Diagram summarizing the molecular interactions regulated by Fzd3 phosphorylation state on T598. HA, human influenza hemagglutinin. IP, immunoprecipitation. Co-IP, coimmunoprecipitation. A.U., arbitrary unit.

regulated (27). In order to detect the intercellular interaction between Fzd3 and Vangl2, we developed a transcellular interaction assay. We transfect Fzd3-HA into HEK cells in one plate with or without Celsr3 and in another plate, Flag-Vangl2 with or without Celsr3. After 24 h of culture, we dissociated and mixed the cells from these two plates together and continued the culture for one more day (Fig. 6A). Using this assay, we were able to detect Fzd3–Vangl2 intercellular interaction using

coimmunoprecipitation (Fig. 6B and C). When Celsr3 was expressed in Fzd3 side or both sides, we observed that the complex formation of intercellular Fzd3–Vangl2 was promoted (Fig. 6B and C).

We then tested whether Fzd3 phosphorylation affects the intercellular interaction between Fzd3 and Vangl2. We found that both Fzd3 T598A and 8A form stronger complexes with Vangl2 than Fzd3WT or Fzd3 7A (Fig. 6D and E). This suggests that

phosphorylation on T598 by LRRK2 negatively regulates the intercellular Fzd3–Vangl2 interaction, while phosphorylation on the other seven sites does not. To further test this, we co-expressed LRRK2 WT, LRRK2 GS, and LRRK2 KN together with Fzd3 in this transcellular interaction assay and found that overexpression of LRRK2 WT and GS caused reduction of Fzd3–Vangl2 interaction but the kinase null LRRK2 did not (Fig. 6 F and G). These results provide more evidence that the

kinase activity of LRRK2 is required for regulating Fzd2–Vangl2 interaction.

To better understand how phosphorylation on T598 may lead to the reduction of Fzd3–Vangl2 interaction, we tested whether and how phosphorylation of T598 on Fzd3 can affect its interaction with Celsr3 in the same cell. We observed that phosphorylation of T598 on Fzd3 is required for a stronger Fzd3–Celsr3 interaction (Fig. 6 H and I), suggesting that a stronger

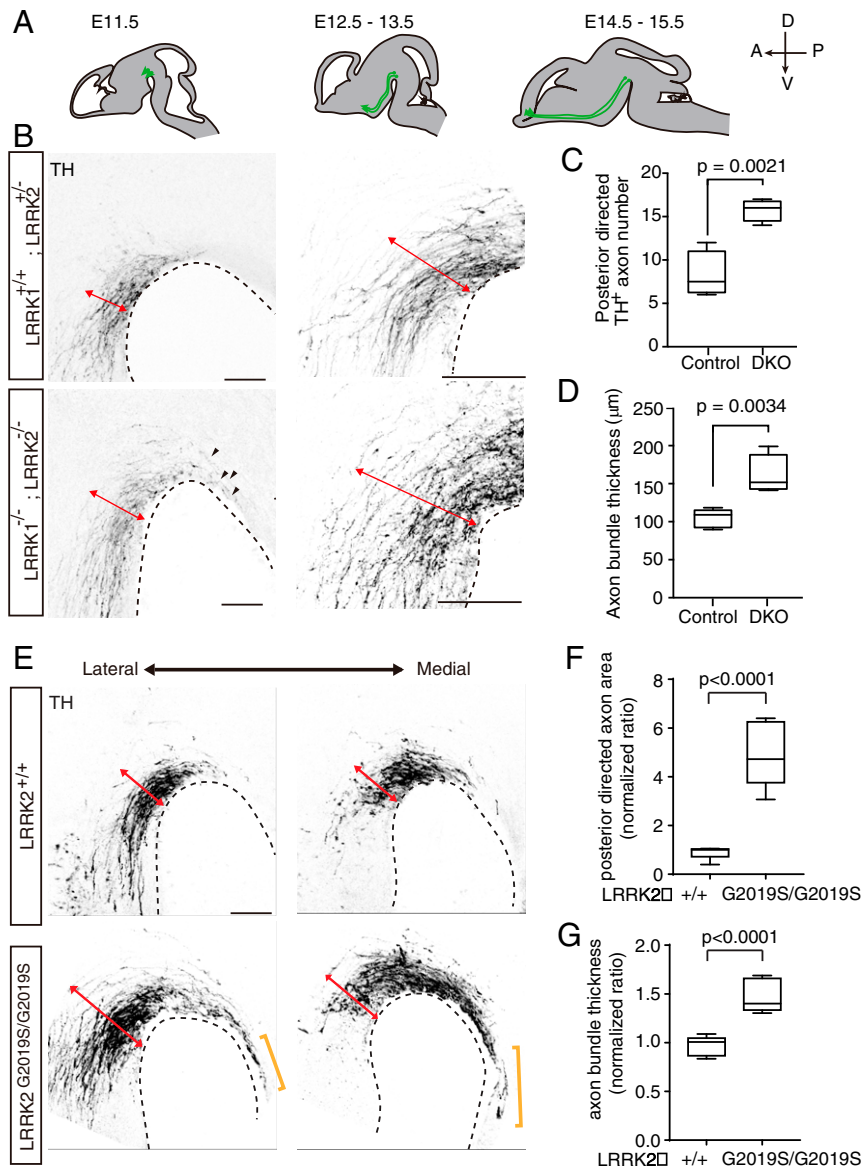


Fig. 7. *LRRK1/2* are required for the proper guidance of mDA axons. (A) A schematic diagram for developmental stages of the mDA axons. mDA (green) emerged at mesencephalic flexure at E11.5 and projected anteriorly and ventrally from E11.5 to E15.5. A, anterior; D, dorsal; P, posterior; V, ventral. (B) mDA axon projections in E12.5 *LRRK1/2* double-knockout and control animals. Sagittal sections were collected from E12.5 embryos and stained for TH. Red arrows indicate the thickness of the mDA axon bundle. Black arrows indicate the mDA axons projecting posteriorly. (Scale bars, 100 μ m.) (C) Quantification of the number of axons targeting posteriorly in B. Data are plotted as Min to Max with median. Min, lowest. Max, highest. Littermates *LRRK1*^{+/+}; *LRRK2*^{+/+} and *LRRK1*^{-/-}; *LRRK2*^{-/-} were used as control. Statistical analyses were done with the Student's *t* test (two-tailed distribution). DKO, *LRRK1*; *LRRK2* double knockout. (D) Quantification of the thickness of the mDA axon bundle. Data are plotted as Min to Max with median. (E) mDA axon projections in E12.5 *LRRK2* GS and WT animals. Sagittal sections were collected from E12.5 embryos and stained for TH. Red arrows indicate the thickness of the mDA axon bundle. Yellow brackets indicate the mDA axons projecting posteriorly. (Scale bars, 100 μ m.) (F) Quantification of area of axons projecting posteriorly in E. Because the number of axons projected posteriorly in GS was much greater than that in *LRRK* loss-of-function mutants, it was not feasible to quantify axon numbers. Therefore, axon areas were quantified here. In WT or GS, three embryos were collected from three different litters. Two serial sagittal sections of mDA were analyzed. TH-positive area posterior to the posterior boundary of the mDA system was analyzed and normalized to the mean of WT littermate. Data are plotted as Min to Max with median. Student's *t* test (two-tailed distribution) was used for statistics. (G) Quantification of axon bundle thickness in E. The thickness of the TH-positive axon bundle was analyzed and normalized to the mean of WT littermate. Data are plotted as Min to Max with median.

Fzd3–Celsr3 intracellular interaction may weaken the intercellular interaction between Fzd3 and Vangl2 (Fig. 6J).

Axon Guidance Defects of Midbrain Dopaminergic (mDA) Neurons in LRRK Mutants. We showed previously that the Wnt–PCP signaling is also essential for anterior-directed growth of mDA axons during embryonic development (13). Moreover, LRRK2 is one of the causal genes of Parkinson’s disease with selective degeneration of the mDA neurons (in substantia nigra pars compacta). It has been reported that LRRK2 is expressed in the embryonic midbrain tyrosine hydroxylase (TH)-positive neurons (49). Therefore, we tested whether LRRK2 is also involved in the development of the mDA axons by analyzing midgestation brains when the mDA axons start to grow anteriorly (E12.5).

In control embryos, the vast majority of the TH-positive mDA axons grow anteriorly in a highly organized way. However, in *LRRK1* and *LRRK2* double knockout, a significant number of mDA axons were found misguided, growing posteriorly (Fig. 7B and C). Moreover, mDA axons in control embryos were normally organized into a compact parallel bundle. We observed that the mDA axon bundle in *LRRK1* and *LRRK2* double knockout was disorganized and much wider (Fig. 7B and D). These results indicate that *LRRK1* and *LRRK2* are also important for the highly organized growth of the mDA axons and proper A–P guidance.

Parkinson’s disease is associated with *LRRK2* gain-of-function mutations. The most frequent mutation is *GS* with enhanced LRRK2 kinase activity. We analyzed the mDA axons in the *GS* knockin embryos. We found that the DA axons also displayed similar axon guidance defects, including widened and disorganized bundle and an increase of posteriorly directed axons (Fig. 7E and G). In fact, the axon guidance defects in *GS* were stronger than *LRRK1/2* double knockout. Therefore, the Parkinson’s disease patients carrying the *GS* mutation may have developmental defects of mDA axon wiring.

Discussion

Growth Cone–Growth Cone Communication as a Guidance Mechanism in Brain Wiring. Axon–axon interactions have long been recognized as an important mechanism in axon guidance (2). For example, differential fasciculation of retinal ganglion cell axons contributes to axon organization prior to target innervation (50). In addition, growth cone–axon interactions are well documented in retinotectal mapping (51). However, whether and how the growth cones interact with each other are not known. Here, we demonstrate the existence of growth cone–growth cone interaction during the collective and directed turning of commissural axons after floor plate turning. This growth cone–growth cone interaction is mediated by the PCP signaling components, specifically through the intercellular interaction between Fzd3 and Vangl2, which is regulated by LRRK2.

Cell–cell interactions in PCP are fundamental for the initiation, amplification, or maintenance of the cell and tissue polarity along the tissue plane (Fig. 8A). We previously showed that, within the same cell, Dvl1 induces Fzd3 hyperphosphorylation and promotes the cell surface localization of Fzd3, whereas Vangl2 inhibits Fzd3 hyperphosphorylation and reduces the cell surface localization of Fzd3. Arf6 promotes the internalization of unphosphorylated Fzd3, which activates c-Jun N-terminal kinase (JNK) through Dvl2 and atypical protein kinase C (aPKC) (14, 17). We now show that, between two neighboring cells, Celsr3 promotes the intercellular interaction of Fzd3 and Vangl2, a key interaction essential for PCP signaling. This Fzd3–Vangl2 intercellular interaction together with the Fzd3–Vangl2 intracellular antagonism may amplify and propagate the planar polarity signal. We also show here that LRRK2 is a key regulator of the Fzd3 phosphorylation state. Together with Dvl1, LRRK2 induces Fzd3 hyperphosphorylation and promotes cell surface accumulation of Fzd3. LRRK2 also directly phosphorylates Fzd3

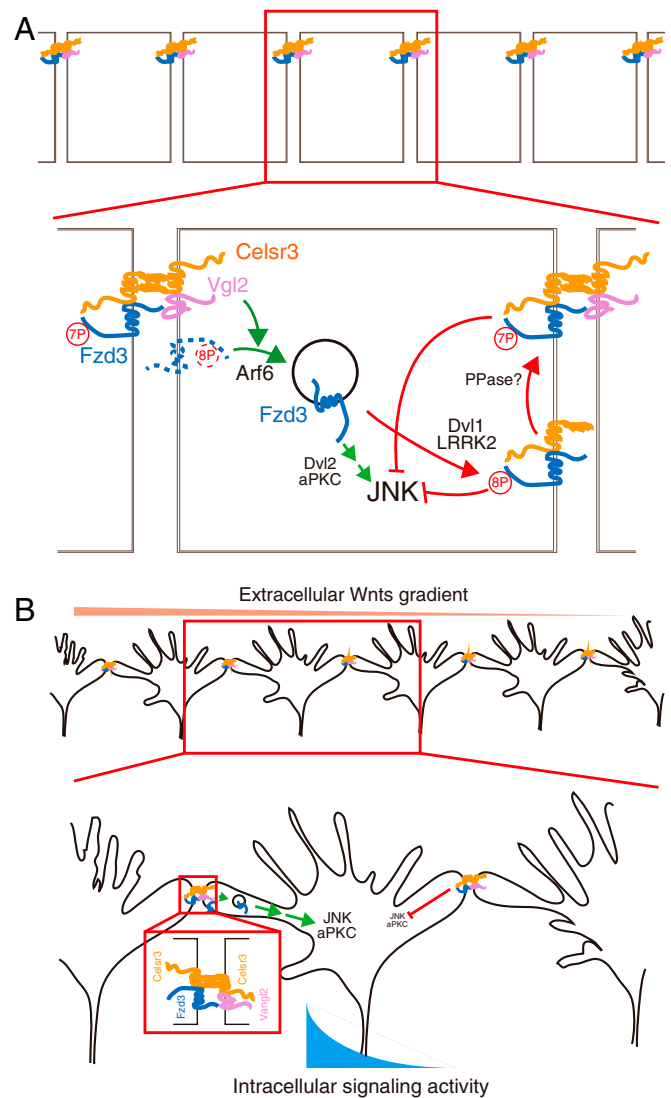


Fig. 8. Schematics of a hypothesis for how PCP signaling components control growth cone turning and mediate growth cone–growth cone communication and a role of LRRK2. (A) A hypothesis for how LRRK2 may regulate cell–cell interactions mediated by PCP components. (B) A hypothesis for how cell–cell interactions mediated by PCP signaling components may regulate growth cone–growth cone communication to increase fidelity. JNK, c-Jun N-terminal kinase. aPKC, atypical protein kinase C. PPase, protein phosphatase.

on T598, which reduces the intercellular interaction between Fzd3 and Vangl2. An unknown protein phosphatase might also be involved here to regulate the Fzd3–Vangl2 transcellular interaction. We hypothesize that the proper level of Fzd3 phosphorylation or a proper sequence of Fzd3 phosphorylation events is critical for the proper cell–cell communication. We propose that kinases, such as LRRK2, and protein phosphatases can regulate the cell–cell communication by regulating Fzd3 phosphorylation state and Fzd3–Vangl2 intercellular interaction.

Our results allow us to propose the following hypothesis of how PCP signaling components may regulate growth cone–growth cone communication. Cohorts of commissural axon growth cones arrive at the floor plate at the same time, cross the midline together, and make a 90° turn anteriorly in a coordinated way (Fig. 8B). As it takes hours for the commissural axons to cross the midline and turn anteriorly, their growth cones would have sufficient time to communicate with each other. In a Wnt

gradient, Fzd3 endocytosis is more active on the side facing higher Wnt concentration where the filopodia growth is enhanced (17). Therefore, the cell surface Fzd3 would be less abundant on the side facing higher Wnt concentration. Vangl2 is enriched at the tips of the growing filopodia and promotes Fzd3 endocytosis more frequently on the side of the growth cones facing higher Wnt concentration. Therefore, the cell surface Vangl2 would be more abundant on the side facing higher Wnt concentration. We hypothesize that this Fzd3–Vangl2 intercellular interaction between the neighboring growth cones, together with the Fzd3–Vangl2 antagonism within the same growth cones, may help amplify and propagate the polarity signal across the growth cones to increase the signaling fidelity. This proposed mechanism may mediate the coordination of a group of growth cones, which exit the floor plate after midline crossing to turn anteriorly together. LRRK2, acting as a scaffold, promotes Fzd3 hyperphosphorylation by recruiting other kinases and Fzd3 cell surface localization. LRRK2 also directly phosphorylates Fzd3 on T598 and negatively regulates the Fzd3–Vangl2 intercellular interaction. Either loss of function of *LRRK2* or a gain of function of *LRRK2 GS* (increased kinase activity) affects the normal growth cone–growth cone interaction and caused axon guidance defects. Therefore, we hypothesize that the proper levels of Fzd3 phosphorylation or a proper sequence of Fzd3 phosphorylation events is essential for proper growth cone–growth cone communication in axon guidance (Fig. 8B).

This growth cone–growth cone interaction for A–P guidance is likely highly restricted to the time after commissural axons have crossed the midline because the key mediator, Fzd3, was shown to be sequestered in the endoplasmic reticulum of commissural neurons by Shisa2 until they have crossed the midline (41). Therefore, we propose that only after commissural axons reached and crossed the midline and after Shh has down-regulated Shisa2 to allow Fzd3 to be trafficked to the surface of the growth cone can PCP signaling be activated and the growth cone–growth cone interactions mediated by Fzd3–Vangl2 occur to mediate coordinated anterior turning (41).

In the developing nervous system, most of the axons path find in groups. We propose that such PCP-mediated mechanisms may be commonly used to coordinate directed axon growth in many parts of the nervous system. This finding suggests a previously unappreciated guidance information that axons may use during the wiring of the nervous system: cell and tissue polarity. Neural epithelia are highly polarized. This polarity of tissue may not only carry directional information but also, organizational information to help create the spatially ordered axon networks.

Genetic Evidence of the Role of Dvls in Axon Guidance. We previously reported that Dvl1 and Dvl3 induce Fzd3 hyperphosphorylation and Vangl2 and Dvl2 antagonizes that (14, 17). Therefore, we proposed that these antagonistic interactions of PCP components are fundamentally important to impart signaling polarity and thus, directionality and may be the biochemical substrates for signal amplification (52–54). Here, we provided genetic evidence that, indeed, both Dvl1 and Dvl3 are functionally redundant and required for the A–P guidance of commissural axons. Furthermore, Dvl2 is also required for the A–P guidance of commissural axons as shown by Dvl2 conditional knockout. The fact that both Dvl1/3 and Dvl2 are required

supports our hypothesis that the antagonism between Dvl1/3 and Dvl2 is important for A–P guidance of commissural axons.

LRRK2 as a Fzd3 Kinase. As Fzd3 phosphorylation is a key event in PCP signaling, understanding how Fzd3 phosphorylation is regulated will provide valuable insights. We report here that LRRK2 directly phosphorylates Fzd3 on T598 and also acts as a scaffold to recruit other kinases to phosphorylate other sites in Fzd3 cytoplasmic domain. The axon guidance defects in *LRRK2* mutants also suggest that proper regulation of Fzd3 phosphorylation state is essential for axon guidance in vivo. Our study currently does not exclude the possibility that other kinases may also phosphorylate Fzd3 on T598 such as in other cellular context. Because LRRK2 has other substrates, we cannot rule out the possibility that some of the axon guidance phenotypes may be caused by the abnormal phosphorylation state of other LRRK2 substrates (55). However, the LRRK2 phenotypes we report here are consistent with the function of LRRK2 as a Fzd3 kinase, important for growth cone–growth cone interaction.

A Role of Parkinson's Disease Gene, LRRK2, in Axon Guidance. *LRRK2* is one of the causal genes for Parkinson's disease (56, 57). The gain-of-function mutation, *GS*, is one of the most frequent *LRRK2* mutations (37, 38). There has not been any correlation between the loss-of-function mutation of *LRRK2* and Parkinson's disease. The biological functions of LRRK2 and mechanisms of pathogenesis of LRRK2 mutations have not been well understood. It has been reported that *LRRK2 GS* mutation alters adult neurogenesis and dendrite outgrowth in vivo and in dissociated cultures (58, 59). We show here that *LRRK2* loss-of-function and *LRRK2 GS* gain-of-function mutations lead to guidance defects of spinal cord commissural axons and the mDA axon during embryonic development. It is currently unclear whether there are axon guidance defects, or transient developmental guidance defects, in Parkinson's disease patients. Although understanding the role of the axon guidance functions of LRRK2 in Parkinson's disease falls outside the scope of this study, the identification of Fzd3 as a LRRK2 substrate may provide an avenue for understanding its biological functions.

Methods

All animal work in this research was approved by the University of California San Diego (UCSD) Institutional Animal Care and Use Committee. Experiments were conducted in accordance with the NIH Guide for the Care and Use of Laboratory Animals and approved by the UCSD Animal Subjects Committee (Approved Protocol # S06219, S06222) (60). A detailed description of all of the methods, data, and statistical analyses is included in *SI Appendix*. Protocols and materials in the paper will be made available to reader upon request.

Data Availability. All of the data are included in the figures and *SI Appendix*.

ACKNOWLEDGMENTS. This work was supported by NIH Grant R37 NS047484 to Y. Z. We thank Z. Xu for sharing the LRRK2 constructs; W. D. Snider, A. Wynshaw-Boris, and A. Alvarez-Buylla for sharing the *Dvl1* knockout, *Dvl3* knockout, and *Dvl2* floxed alleles; E. Kothari and J. Zhao of the University of California San Diego (UCSD) Transgenic core for injecting sgRNA/Cas9 mRNA to make the LRRK1 and LRRK2 CRISPR knockout lines; M. Ghasseman of the UCSD Biomolecular and Proteomics Mass Spectrometry Facility for identifying the Fzd3 phosphorylation site by LRRK2; and J. Santini of the UCSD School of Medicine Light Microscopy Facility (Grant P30 NS047101) for assistance with microscopy.

1. E. T. Stoeckli, Understanding axon guidance: Are we nearly there yet? *Development* **145**, dev151415 (2018).
2. L. Wang, T. Marquardt, What axons tell each other: Axon-axon signaling in nerve and circuit assembly. *Curr. Opin. Neurobiol.* **23**, 974–982 (2013).
3. A. I. Lyuksyutova et al., Anterior-posterior guidance of commissural axons by Wnt-frizzled signaling. *Science* **302**, 1984–1988 (2003).
4. S. Yoshikawa, R. D. McKinnon, M. Kokel, J. B. Thomas, Wnt-mediated axon guidance via the *Drosophila* Derailed receptor. *Nature* **422**, 583–588 (2003).
5. Y. Liu et al., Ryk-mediated Wnt repulsion regulates posterior-directed growth of corticospinal tract. *Nat. Neurosci.* **8**, 1151–1159 (2005).

6. A. M. Schmitt et al., Wnt-Ryk signalling mediates medial-lateral retinotectal topographic mapping. *Nature* **439**, 31–37 (2006).
7. M. Sato, D. Umetsu, S. Murakami, T. Yasugi, T. Tabata, DWnt4 regulates the dorsoventral specificity of retinal projections in the *Drosophila melanogaster* visual system. *Nat. Neurosci.* **9**, 67–75 (2006).
8. C. L. Pan et al., Multiple Wnts and frizzled receptors regulate anteriorly directed cell and growth cone migrations in *Caenorhabditis elegans*. *Dev. Cell* **10**, 367–377 (2006).
9. M. A. Hilliard, C. I. Bargmann, Wnt signals and frizzled activity orient anterior-posterior axon outgrowth in *C. elegans*. *Dev. Cell* **10**, 379–390 (2006).

10. B. C. Prasad, S. G. Clark, Wnt signaling establishes anteroposterior neuronal polarity and requires retromer in *C. elegans*. *Development* **133**, 1757–1766 (2006).
11. T. R. Keeble *et al.*, The Wnt receptor Ryk is required for Wnt5a-mediated axon guidance on the contralateral side of the corpus callosum. *J. Neurosci.* **26**, 5840–5848 (2006).
12. E. Domanitskaya *et al.*, Sonic hedgehog guides post-crossing commissural axons both directly and indirectly by regulating Wnt activity. *J. Neurosci.* **30**, 11167–11176 (2010).
13. A. G. Fenstermaker *et al.*, Wnt/planar cell polarity signaling controls the anterior-posterior organization of monoaminergic axons in the brainstem. *J. Neurosci.* **30**, 16053–16064 (2010).
14. B. Shafer, K. Onishi, C. Lo, G. Colakoglu, Y. Zou, Vangl2 promotes Wnt/planar cell polarity-like signaling by antagonizing Dvl1-mediated feedback inhibition in growth cone guidance. *Dev. Cell* **20**, 177–191 (2011).
15. K. Shimizu, M. Sato, T. Tabata, The Wnt5/planar cell polarity pathway regulates axonal development of the *Drosophila* mushroom body neuron. *J. Neurosci.* **31**, 4944–4954 (2011).
16. E. M. Mrkusic, D. J. Flanagan, P. M. Whittington, The core planar cell polarity gene *prickle* interacts with *flamingo* to promote sensory axon advance in the *Drosophila* embryo. *Dev. Biol.* **358**, 224–230 (2011).
17. K. Onishi *et al.*, Antagonistic functions of *Dishevelleds* regulate *Frizzled3* endocytosis via filopodia tips in Wnt-mediated growth cone guidance. *J. Neurosci.* **33**, 19071–19085 (2013).
18. E. Huarcaya Najarro, B. D. Ackley, *C. elegans* *fmi-1/flamingo* and Wnt pathway components interact genetically to control the anteroposterior neurite growth of the VD GABAergic neurons. *Dev. Biol.* **377**, 224–235 (2013).
19. R. Gombos *et al.*, The formin DAAM functions as molecular effector of the planar cell polarity pathway during axonal development in *Drosophila*. *J. Neurosci.* **35**, 10154–10167 (2015).
20. E. C. Avilés, E. T. Stoeckli, Canonical wnt signaling is required for commissural axon guidance. *Dev. Neurobiol.* **76**, 190–208 (2016).
21. V. Leung *et al.*, The planar cell polarity protein Vangl2 is required for retinal axon guidance. *Dev. Neurobiol.* **76**, 150–165 (2016).
22. S. D. Sun, A. M. Purdy, G. S. Walsh, Planar cell polarity genes *Frizzled3a*, *Vangl2*, and *Scribble* are required for spinal commissural axon guidance. *BMC Neurosci.* **17**, 83 (2016).
23. M. T. Butler, J. B. Wallingford, Planar cell polarity in development and disease. *Nat. Rev. Mol. Cell Biol.* **18**, 375–388 (2017).
24. A. C. Humphries, M. Mlodzik, From instruction to output: Wnt/PCP signaling in development and cancer. *Curr. Opin. Cell Biol.* **51**, 110–116 (2018).
25. C. Zheng, M. Diaz-Cuadros, M. Chalfie, *Dishevelled* attenuates the repelling activity of Wnt signaling during neurite outgrowth in *Caenorhabditis elegans*. *Proc. Natl. Acad. Sci. U.S.A.* **112**, 13243–13248 (2015).
26. C. H. Chen, C. W. He, C. P. Liao, C. L. Pan, A Wnt-planar polarity pathway instructs neurite branching by restricting F-actin assembly through endosomal signaling. *PLoS Genet.* **13**, e1006720 (2017).
27. J. Wu, M. Mlodzik, The frizzled extracellular domain is a ligand for Van Gogh/Stbm during nonautonomous planar cell polarity signaling. *Dev. Cell* **15**, 462–469 (2008).
28. R. M. Sancho, B. M. Law, K. Harvey, Mutations in the LRRK2 Roc-COR tandem domain link Parkinson's disease to Wnt signalling pathways. *Hum. Mol. Genet.* **18**, 3955–3968 (2009).
29. J. C. Dächsel *et al.*, Identification of potential protein interactors of *Lrrk2*. *Parkinsonism Relat. Disord.* **13**, 382–385 (2007).
30. A. K. Liou, R. K. Leak, L. Li, M. J. Zigmond, Wild-type LRRK2 but not its mutant attenuates stress-induced cell death via ERK pathway. *Neurobiol. Dis.* **32**, 116–124 (2008).
31. S. Zach, S. Felk, F. Gillardon, Signal transduction protein array analysis links LRRK2 to Ste20 kinases and PKC zeta that modulate neuronal plasticity. *PLoS One* **5**, e13191 (2010).
32. E. Ohta, F. Kawakami, M. Kubo, F. Obata, LRRK2 directly phosphorylates Akt1 as a possible physiological substrate: Impairment of the kinase activity by Parkinson's disease-associated mutations. *FEBS Lett.* **585**, 2165–2170 (2011).
33. P. Gómez-Suaga *et al.*, Leucine-rich repeat kinase 2 regulates autophagy through a calcium-dependent pathway involving NAADP. *Hum. Mol. Genet.* **21**, 511–525 (2012).
34. F. Kawakami *et al.*, Leucine-rich repeat kinase 2 regulates tau phosphorylation through direct activation of glycogen synthase kinase-3 β . *FEBS J.* **281**, 3–13 (2014).
35. L. Parisiadou *et al.*, LRRK2 regulates synaptogenesis and dopamine receptor activation through modulation of PKA activity. *Nat. Neurosci.* **17**, 367–376 (2014).
36. E. Kinoshita, E. Kinoshita-Kikuta, K. Takiyama, T. Koike, Phosphate-binding tag, a new tool to visualize phosphorylated proteins. *Mol. Cell. Proteomics* **5**, 749–757 (2006).
37. E. Greggio, M. R. Cookson, Leucine-rich repeat kinase 2 mutations and Parkinson's disease: Three questions. *ASN Neuro* **1**, e00002 (2009).
38. J. H. Kluss *et al.*, Detection of endogenous S1292 LRRK2 autophosphorylation in mouse tissue as a readout for kinase activity. *NPJ Parkinsons Dis.* **4**, 13 (2018).
39. A. L. McCormack *et al.*, Direct analysis and identification of proteins in mixtures by LC/MS/MS and database searching at the low-femtomole level. *Anal. Chem.* **69**, 767–776 (1997).
40. H. Steen, J. A. Jebanathirajah, J. Rush, N. Morrice, M. W. Kirschner, Phosphorylation analysis by mass spectrometry: Myths, facts, and the consequences for qualitative and quantitative measurements. *Mol. Cell. Proteomics* **5**, 172–181 (2006).
41. K. Onishi, Y. Zou, Sonic Hedgehog switches on Wnt/planar cell polarity signaling in commissural axon growth cones by reducing levels of *Shisa2*. *eLife* **6**, e25269 (2017).
42. E. Giaime *et al.*, Age-dependent dopaminergic neurodegeneration and impairment of the autophagy-lysosomal pathway in LRRK-deficient mice. *Neuron* **96**, 796–807.e6 (2017).
43. O. Avraham *et al.*, Transcriptional control of axonal guidance and sorting in dorsal interneurons by the Lim-HD proteins *Lhx9* and *Lhx1*. *Neural Dev.* **4**, 21 (2009).
44. T. S. Tran *et al.*, *Neuropilin2* regulates the guidance of post-crossing spinal commissural axons in a subtype-specific manner. *Neural Dev.* **8**, 15 (2013).
45. F. Charron, E. Stein, J. Jeong, A. P. McMahon, M. Tessier-Lavigne, The morphogen sonic hedgehog is an axonal chemoattractant that collaborates with *netrin-1* in midline axon guidance. *Cell* **113**, 11–23 (2003).
46. Y. Matsumoto, F. Irie, M. Inatani, M. Tessier-Lavigne, Y. Yamaguchi, *Netrin-1/DCC* signaling in commissural axon guidance requires cell-autonomous expression of heparan sulfate. *J. Neurosci.* **27**, 4342–4350 (2007).
47. S. Ohata *et al.*, Loss of *Dishevelleds* disrupts planar polarity in ependymal motile cilia and results in hydrocephalus. *Neuron* **83**, 558–571 (2014).
48. Y. Wang, J. Nathans, Tissue/planar cell polarity in vertebrates: New insights and new questions. *Development* **134**, 647–658 (2007).
49. B. S. Han *et al.*, Expression of the LRRK2 gene in the midbrain dopaminergic neurons of the substantia nigra. *Neurosci. Lett.* **442**, 190–194 (2008).
50. A. A. Sitko, T. Kuwajima, C. A. Mason, Eye-specific segregation and differential fasciculation of developing retinal ganglion cell axons in the mouse visual pathway. *J. Comp. Neurol.* **526**, 1077–1096 (2018).
51. J. A. Raper, E. B. Grunewald, Temporal retinal growth cones collapse on contact with nasal retinal axons. *Exp. Neurol.* **109**, 70–74 (1990).
52. Y. Zou, Does planar cell polarity signaling steer growth cones? *Curr. Top. Dev. Biol.* **101**, 141–160 (2012).
53. K. Onishi, E. Hollis, Y. Zou, Axon guidance and injury-lessons from Wnts and Wnt signaling. *Curr. Opin. Neurobiol.* **27**, 232–240 (2014).
54. Y. Zou, Breaking symmetry: Cell polarity signaling pathways in growth cone guidance and synapse formation. *Curr. Opin. Neurobiol.* **63**, 77–86 (2020).
55. T. Kuwahara, T. Iwatsubo, The emerging functions of LRRK2 and Rab GTPases in the endolysosomal system. *Front. Neurosci.* **14**, 227 (2020).
56. C. Paísán-Ruiz *et al.*, Cloning of the gene containing mutations that cause PARK8-linked Parkinson's disease. *Neuron* **44**, 595–600 (2004).
57. A. Zimprich *et al.*, Mutations in LRRK2 cause autosomal-dominant parkinsonism with pleomorphic pathology. *Neuron* **44**, 601–607 (2004).
58. N. J. Lavalley, S. R. Slone, H. Ding, A. B. West, T. A. Yacoubian, 14-3-3 Proteins regulate mutant LRRK2 kinase activity and neurite shortening. *Hum. Mol. Genet.* **25**, 109–122 (2016).
59. B. Winner *et al.*, Adult neurogenesis and neurite outgrowth are impaired in LRRK2 G2019S mice. *Neurobiol. Dis.* **41**, 706–716 (2011).
60. National Research Council, *Guide for the Care and Use of Laboratory Animals*, (National Academies Press, Washington, DC, ed. 8, 2011).